AUTOMATIC MAPPING OF LUNAR CRATERS AND BOULDERS. Andres Huertas and Yang Cheng, Jet Propulsion Laboratory, California Institute of Technology, Pasadena, CA 91109.

Introduction: The availability of high-resolution images of the surface of the Moon makes it possible to fully resolve boulders and craters as small as 5 pixels in diameter. At the nominal resolution of the Narrow Angle Cameras (NAC) on board the Lunar Reconnaissance Orbiter (LRO) this translates into 2.5 meters. As part of the Lunar Mapping and Modeling Project (LMMP) managed by NASA's Marshall Space Flight Center, we are applying automatic algorithms for the detection and mapping of boulders and craters for 25 regions of interest (ROI) on the lunar surface. These algorithms have reached a high level of maturity over the last few years, and have been adapted to the lunar environment. We give a brief description of the algorithms and present results from one ROI located at the South Pole Aitken Basin Interior (SPABI). A non-projected NAC image (5,064x52,224 pixels) typically covers an area of 2.5km x26km. Our goal is to detect, map, and describe the statistics of detected boulders and craters for all 25 ROIs within one year. Identifying which craters and boulders, together with small scale slope and roughness estimates, leads to construction of hazard maps that can be used for various types of analysis for lunar missions that include landers, rovers and walkers. These mapping products, together with data from other sensors (digital elevation models (DEM), resource maps, surface lighting availability, and others) are planned to be accessible on-line through the LMMP portal, under development, in about one year.

Surface Rocks: The technology to detect rocks automatically during the final stage of descent on a planetary surface was developed at JPL several years ago to provide on-board hazard detection and avoidance, in real-time, using a single descent camera image [1]. The detector relies on knowledge of the Sun angles to analyze the shadows in the image that may correspond to surface rocks (and similar features) to estimate their diameters. With the loose assumption that the local terrain is leveled, the rock heights are also estimated. The smallest shadow region analyzed is 5 image pixels. The algorithm was enhanced in 2007 to map rocks acquired by the HiRISE (nominally 0.3m/pixel) camera on board the Mars Reconnaissance Orbiter (MRO) for the Phoenix mission [2,3] and currently for the Mars Science Laboratory, scheduled for launch in 2011. A version of the algorithm has been adapted to the lunar environment, by allowing, for example, to distinguish shadows from small craters to those cast by surface boulders, and also to adapt to the changing contrast of the shadow regions in locally undulating terrain and shading of large eroded crater walls. In terms of performance, we anticipate that at least 85% of boulders will be detected. For scenes acquired with low Sun angles the boulder shadows may become merged and thus difficult to discern. All rocks detected, however, would be hazardous to a lander, which may have roughness tolerances as low as 0.3m. On the average, the rocks height/diameter ratio is 0.5, and at that translates into 0.6m diameter rocks. Rocks below full resolvability (2.5m) are detected in smaller numbers and must eventually be accounted for by updated statistical models of lunar rock abundance. The smallest detectable rock is ~1.2m diameter.

Craters: The algorithms for automatic crater detection at JPL have been evolving for a decade. Craters are salient features on planetary and small bodies. Mapped craters initially focused on sharp craters with robust detections useful for orbit determination and for terrain relative navigation (TRN) [4,5]. For LMMP, and potential future projects, the crater detection algorithm has been substantially enhanced to locate and map eroded craters as well. Further, the algorithm uses basic assumptions about the terrain and surface albedo near craters to estimate the slope of the crater interior and walls. This feature is useful when a local DEM is not available, and to characterize the hazardousness of craters for landed missions. Preliminary performance evaluation indicates that at least 85% of the craters in a NAC image can be identified. Using a measure of rim sharpness last summer, about 98% of hazardous craters were identified. A combination of crater and boulder detection results also yields a first approximation to the relationship between craters and boulders on the lunar surface. While most boulders in the SPABI appear to concentrate inside and around craters, not all craters of a given size have boulders, and some boulders are not near large craters. These relationships hence provide a rich source of analyses of the large number of secondary craters and the local depth of the regolith.

Results: Fig. 1 illustrates as 11 NAC images overlaid on an LRO's WAC (wide angle camera) image and covering ~400km^2 at the SPABI ROI. NAC images are acquired by two cameras (designated L and R, but are not stereo pairs.) In our work we use calibrated images that have been de-noised to reduce the sensor pattern noise present in the original images. We also use non-projected images to avoid distortion and smear of the smallest features if interest (rocks.) Fig 2 & Fig3 show rock detection and mapping results and preliminary statistics. Note that buried rocks that do not cast dis-

cernable shadows even at a low sun angle are thus not detected but also not hazardous.

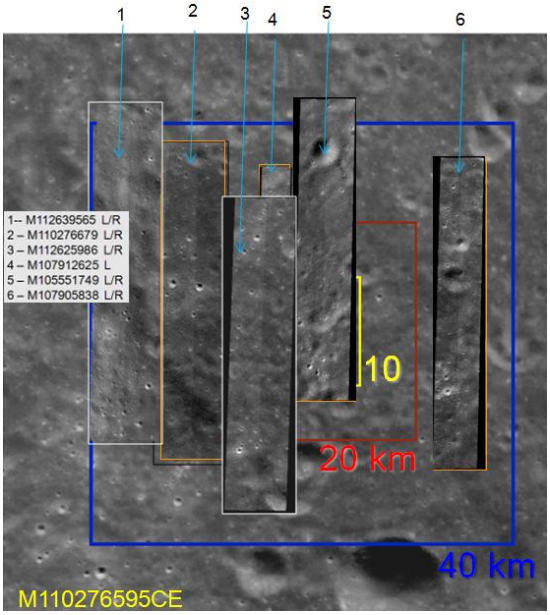

Fig 1. Eleven NAC images of the SPABI region used to map craters and boulders in the LMMP project.

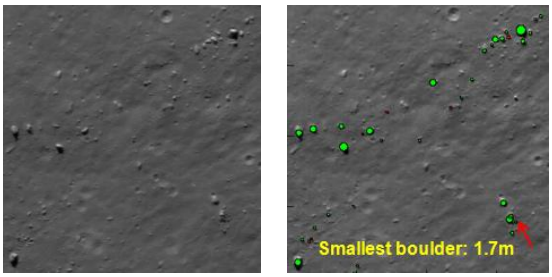

Fig 2. 210m x 210m sub-window of NAC M110276679RC with detected boulder models illustrated by red and green circles.

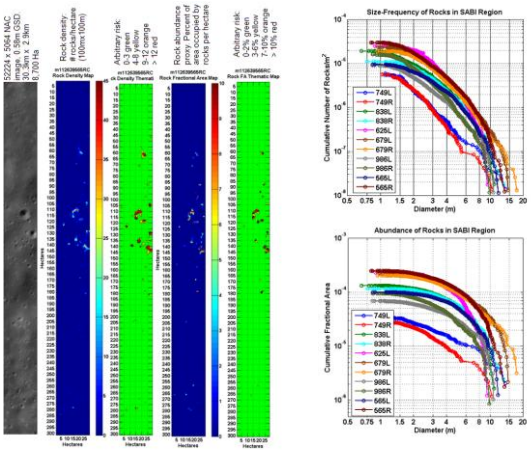

Fig 3. NAC image M112539565RC, a rock density map (# rocks/ha), a thematic rock density map shows landing risk, a rock fractional area map (% of ha occupied by rocks). Size-frequency distribution and rock abundance plots for the eleven images in SPABI.

Fig. 4 & Fig. 5 show crater detection and mapping results and preliminary basic statistics.

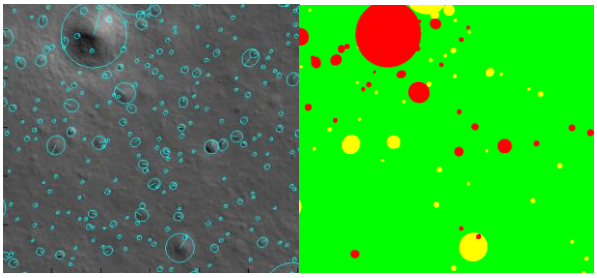

Fig. 4. Craters detected in 84m x 80m sub-image of NAC M105551749LC (left). Most of the craters in this example are eroded and as small as 2.5m diameter. Average crater wall slopes estimated across the craters along the projection of the sun rays by shading analysis identifies potential hazard to landers. Red craters have slopes > 15^{o}. Craters in green area have slopes < 11^{o}. Yellow craters are in between.

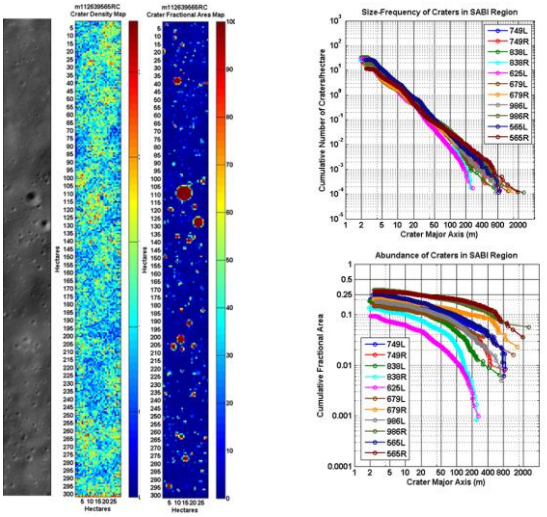

Fig. 4. NAC image M112539565RC, a crater density map (# craters/ha), a rock fractional area map (% of ha occupied by craters). Size-frequency distribution and crater abundance plots for the eleven images in the SPABI region.

References: [1] A. Huertas, Y. Cheng & R. Madison (2006), *IEEE Aerospace Conf. Proc*. [2] M. Golombek, A. Huertas, et.al. (2008). *JGR 113(E00A09)*. [3] M. Golombek, H. Sizemore, A. Huertas, L. Tamppari & M. Mellon (2008) *LPSC XXXIX, Abs.#1868.* [4] Y. Cheng & A. Ansar (2005) *IEEE Int. Conf. Robotics & Autom.*[5] A. Ansar & Y. Cheng (2005) *PE&RS 71, (10).*